A STUDY OF CONFORMAL METASURFACES ON PASSIVE BEAM STEERING FOR ARRAYS

A Dissertation
Submitted to the Graduate Faculty
of the
North Dakota State University
of Agriculture and Applied Science

By

Ruisi Ge

In Partial Fulfillment of the Requirements
for the Degree of
DOCTOR OF PHILOSOPHY

Major Department:
Electrical and Computer Engineering

March 2022

Fargo, North Dakota

North Dakota State University
Graduate School

Title

A STUDY OF CONFORMAL METASURFACES ON PASSIVE BEAM STEERING FOR ARRAYS

By

Ruisi Ge

The Supervisory Committee certifies that this ***disquisition*** complies with North Dakota State University's regulations and meets the accepted standards for the degree of

DOCTOR OF PHILOSOPHY

SUPERVISORY COMMITTEE:

Benjamin Braaten
Chair

Jacob Glower

Qifeng Zhang

Mijia Yang

Approved:

March 2, 2022 — Date

Benjamin Braaten — Department Chair

ABSTRACT

Beam-steering has drawn significant interest due to the expansion of network capacity. However, a traditional beam steering system involves active phase shifters and controlling networks which can be complex. This work proposes a passive conformal metasurface design on beam steering. The phase shifting is achieved by changing the curvature of a conformal metasurface. In addition, three conformal prototypes were fabricated and tested using different techniques such as 3D printing. The simulations and test results indicate up to 20° of beam shifting. This study can be extended to higher frequency bands for lower power consumption beam steering systems.

ACKNOWLEDGMENTS

I am very grateful to take this chance to thanks Dr. Braaten, Dr. Glower , Dr. Zhang and Dr. Yang for serving on my graduate committee. Dr. Braaten was my master's and Ph.D. advisor in electromagnetics . I can not thank him enough for his patience, wisdom, and guidance during my studies. He has shown me the importance of teaching, awards of research., and most importantly, optimistic attitude towards life.

I would like to thank Dr. Glower, Dr. Zhang and Dr. Yang for serving on my graduate committee. I have enjoyed the discussions in engineering and research topics with these professors and look forward for future discussions and collaboration.

I would especially like to thank Ryan Striker, my lab mate and fellow Ph.D. student who research with me on the project. His skills in fabricating provided me with another perspective on this research. I also enjoyed the discussions on various aspect of the project.

Finally, I would like to thank my family for their support of my Ph.D. studies.

DEDICATION

To my family.

TABLE OF CONTENTS

LIST OF TABLES

LIST OF FIGURES

1. INTRODUCTION

1.1. Beam steering and previous studies

In recent years, beam-steering has garnered significant interest in the antenna design community due to the development of 5G wireless networks. Compared with 4G wireless communications, the potential 5G wireless networks will provide more wireless capacity [1]. The dramatic increase of capacity and utilization of higher frequency bands brings a lot of challenges for antenna design. One of the most promising techniques to overcome those challenges is beam steering. A traditional active beam steering system is shown in Figure 1.[2].

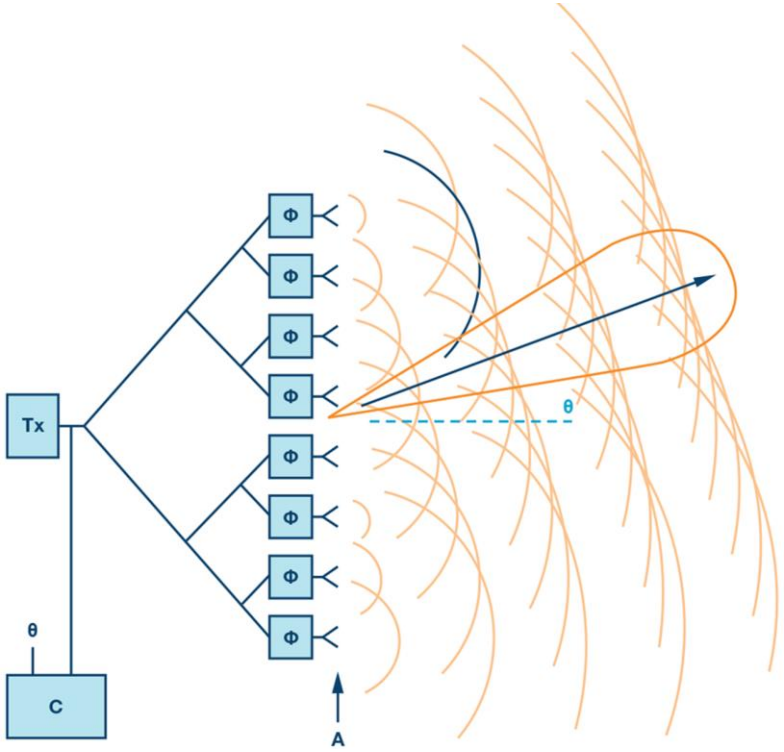

Figure 1. Active beam steering [2].

Active phase shifters were used to change the phase of each radiating element of the array. By tuning phase shifters of different elements, the direction of the main lobe of a radiation pattern can be changed, therefore the beam can be guided to a desired direction. Compared with the single element antenna, phased arrays can adjust the signal and combine multiple elements, therefore

enhance the overall performance including gain improvement. The concept of beam steering and phased arrays is not new, but with the development of 5G networks pushing to higher frequencies, antennas are required to overcome higher path loss. Furthermore, the shorter wavelength translates into smaller antennas, which makes phased arrays and beam steering more feasible for commercial products. Thus, beam steering became one of the most promising technique for antenna designs in 5G networks.

There are also multiple challenges for active beam steering and phased array antennas. Phased array antennas usually involve synthesis of multiple elements and controlling circuits which make the system complex and harder to fabricate. Moreover, multiple active phase shifters also add cost and power consumption to the overall system [3]. Therefore, some researchers start to explore low cost and low power consumption solutions.

There are many researchers trying to explore different methods to achieve beam steering without implementing active phase shifters in the power source. Methods include antenna designs based on coding intelligent surfaces [4-7], tunable materials [8-15], conformal surfaces [16-20] etc. In [21], A reconfigurable transmit-array was used for beam steering and polarization. The transmit-array element consisted of an active side, reflective phase shifters, and a passive side. With a tunable active patch structure and two layers of passive patch structures, beam steering with a scan range of 60 degree at 5.4 GHz was achieved. A wide range of beam steering was achieved by utilizing active patch structures instead of an active phase shifter. However, the complex structure of multiple layer structures also adds to the difficulty and cost.

In [22], a phase-gradient metasurface was proposed to control the most significant grating lobes in two-dimensional beam-steering systems. By rotating a pair of phase-gradient metasurfaces (PGMs), high directivity could be achieved. This research further proposed to reduce the

undesirable dominant grating lobes by optimizing a supercell and increase the transmission phase gradient of PGMS. However, this method is complex and increases the manufacturing complexity with multi-layer phase gradients.

1.2. Metasurfaces and previous studies

One method to increase the beam steering range is to utilize a metasurface. Metamaterials are composed of periodic structures that resonantly couple to the electric and magnetic components of the incident electromagnetic fields [23]. However, due to the high losses with the resonant responses and the difficulty in fabricating the microscale 3D structures for metamaterials, metasurfaces become a more practical approach for antenna design. Metasurfaces, consisting of single-layer or several-layer stacks of planar structures can be readily fabricated, and the ultrathin thickness in the wave propagation direction creates less undesirable losses [24,25]. Each unit cell of the metasurface is regarded as an electrically small antenna that receives power from illuminated waves and reemits waves to form reflected/transmitted wave fronts [26]. An overview of the metasurface is shown in the Figure 2 [27].

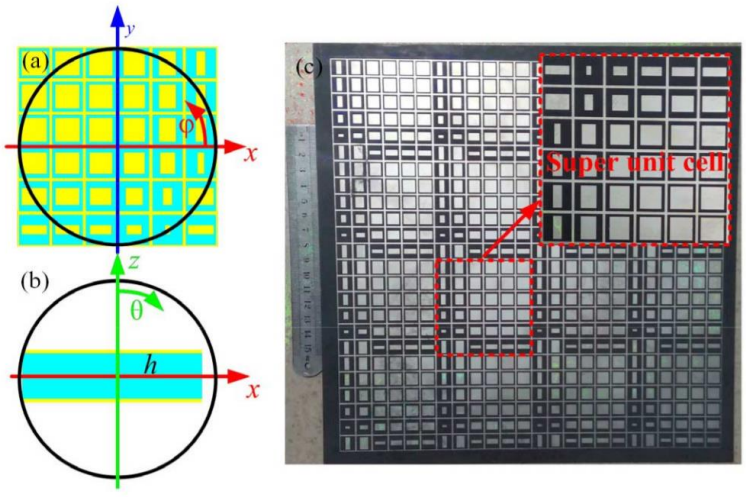

Figure 2. Overview of a phase-gradient metasurface[27].

Many research groups dedicate their studies to metasurfaces due to its distinctive properties. Metasurfaces are used for gain enhancement [28], bandwidth improvement [29], phase error rectification [30] and radiation pattern reconfiguration [31]. Moreover, by properly manipulating the incident, reflected and transmitted field, certain desired wave transformations can be realized. Metasurface can be use as artificial magnetic conductors [32], spatial filters [33], and transit arrays [34].

In [35], a frequency-reconfigurable antenna was designed using metasurfaces. The metasurface consists of rectangular-loop unit cells placed periodically in the vertical and horizontal directions. Measured results show that the antenna has a tuning range from 4.76 to 5.51 GHz. Radiation efficiency and a realized peak gain of more than 80% and 5 dBi was achieved. In [36], the single and dual layer metasurfaces are proposed to miniaturize a low-profile wideband antenna. The metasurfaces consisted of one and two square patch arrays, with the increased effective refractive index, both the proposed antennas realize a gain greater than 6.5 dBi. In [37], Beam steering was achieved by transforming phase of the antenna near field using a pair of totally passive metasurfaces. Metasurfaces are rotated independently or synchronously around the antenna axis. A prototype was fabricated to demonstrate experimentally that the beam of a resonant cavity antenna can be steered. Those studies demonstrated that metasurfaces can be great candidates for gain improvement and beam steering.

1.3. Conformal antenna and previous studies

Figure 3 shows an example of conformal antenna for wide beam coverage. Compared to planar structures, conformal antenna arrays have an overall wider beam than the planar structure [38]. Placing radiating elements on a conformal surface can increase the beam steering range of the phased array. In [39], a self-adapting conformal antenna for changing spherical surfaces are

studied, the phase compensation expressions were validated experimentally at 2.47 GHz with a precisely controlled 4x4 phased-array antenna attached to conformal surfaces. Different radius conformal surfaces were used to validate the expressions.

In [40], an active conformal metasurface lens was proposed. Microwave varactors were integrated to change the transmission phase of the cylindrical metasurface up to 195 degrees. By increasing the number of feeding sources, the beam steering range of conformal lenses can be expanded to 60 degrees. Without a complex feeding network, the conformal metasurface can be manufactured easily with relatively low cost. Compared with other reconfigurable planar antennas, this antenna has a large scanning range and lower side lobes. However, the conformal metasurface lens still needs to be controlled by a dc bias voltage, and it's not ideal for low power applications.

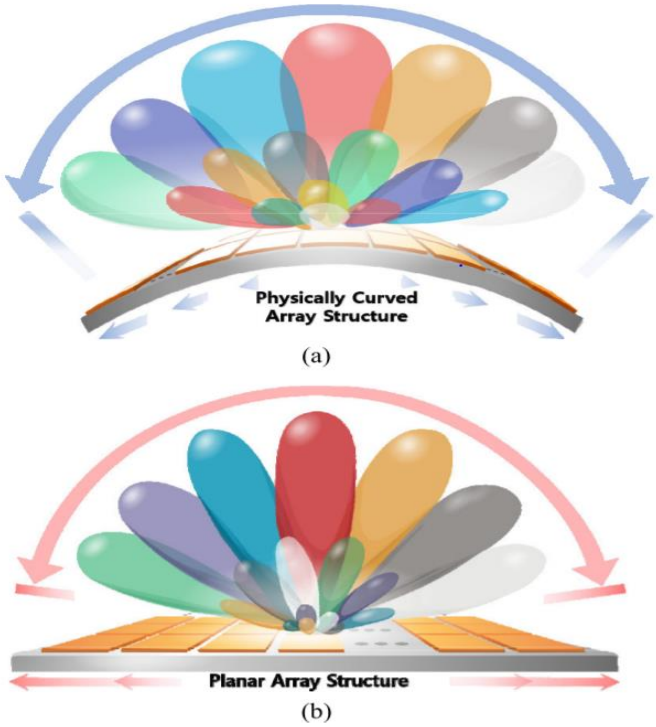

Figure 3. Beam angle comparison between planar and conformal array (a) Curved array structure (b) Planar array structure [38].

2. THE PROPOSED RESEARCH

In this work, we design and demonstrate different passive conformal metasurfaces for beam steering, where each of the passive metasurfaces are placed near a conventional patch antenna as a parasitic element. The overview of the conformal metasurface is shown at the Figure 4. The conformal metasurface design has been simulated and manufactured by three different materials and manufacturing methods.

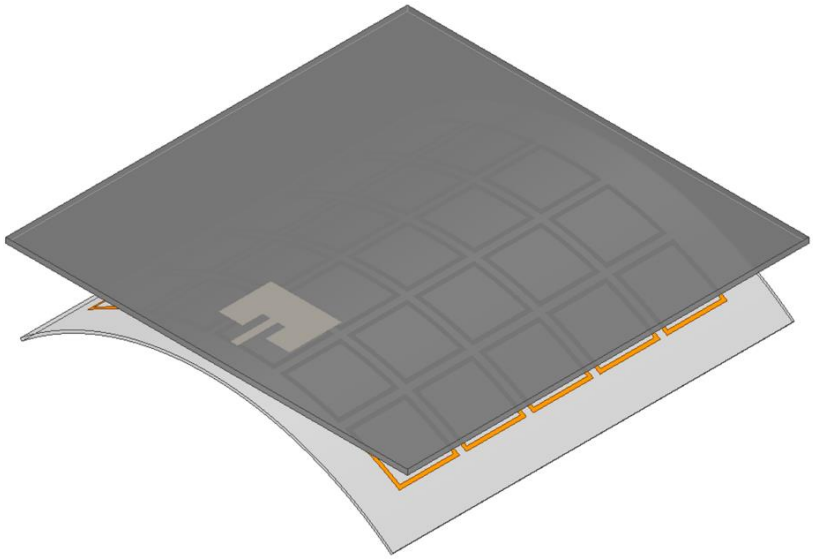

Figure 4. Overview of the conformal metasurface.

Three conformal metasurfaces are:(1). A laser etched Rogers 5883 conformal metasurface, (2). A 3D Printing Ninja flex conformal metasurface, and (3). A Panasonic Felios F775 flexible PCB conformal metasurface. Then the three metasurfaces have been placed on surfaces with different curvatures. When the curvature of the metasurface changes, the inducing electromagnetic fields are altered, therefore the phase of the radiating element has been changed. Finite element-based simulation via HFSS was used to analyzed and demonstrate the performance of the proposed metasurface. Lab test results further verified the effectiveness of the proposed method. The

measured results showed a range of 20 degrees and a 2.7 dB gain increase with a passive and simple structure.

2.1. Theoretical model

To effectively achieve passive beam steering, it's necessary to understand the phase compensation algorithm of a linear array on a conformal surface. In [39],the radiation pattern of a 1 x 4 microstrip antenna array attached to different conformal surfaces was studied. An overview of phase compensation of a linear array on a cylinder shaped conformal metasurface is shown in Figure 5.

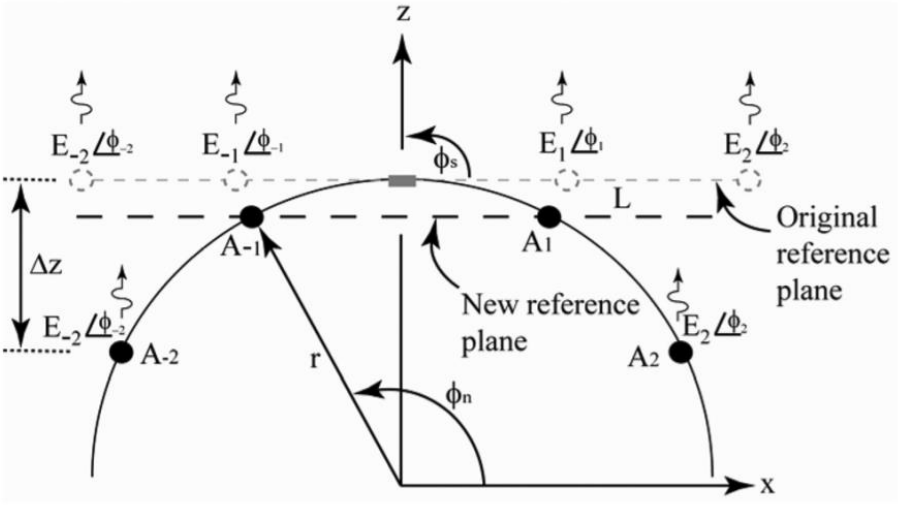

Figure 5. Overview of a phase compensation of a linear array on a single curved surface[39].

By denoting the position of the n^{th} element in the array as (r, ϕ_n), The required phase compensation can be computed as:

$$\Delta\phi_n^c = +kr|\sin(\phi_n) - \sin(\phi_{n-1})| \quad (1)$$

where k is the free-space wave number , r is the radius of the cylinder. The expression assumes that the scanning angle will be 90 degrees. To analytically compute the compensated radiation pattern and validate the measurements of the antenna test platform on the conformal surfaces, the following compensated array factor AF_c was used[39]:

$$AF = AFe^{j\Delta\phi_n} \quad (2)$$

Where ϕ_n is the phase compensation term for the free-space phase delay computed using (1), and array factor (AF) for an antenna conformal surface is[39]:

$$AF = \sum_{n=1}^{N} w_n e^{jk[x_n(u-u_s)+y_n(v-v_s)+z_n\cos\theta]}. \quad (3)$$

Equation (3) assumes a spherical coordinate system where $u = \sin\theta\cos\phi$, $u_s = \sin\theta_s\cos\phi_s$, $v = \sin\theta\sin\phi$, $v_s = \sin\theta_s\sin\phi_s$, θ_s is the elevation steering angle, ϕ_s is the azimuth steering angle, and w_n is the complex weighting function.

When designing phased arrays and leaky wave antennas, array factor calculations [41] inform the beam synthesis process. These methods provide weightings for each of the radiating elements along the aperture to achieve a beam in a desired direction. However, independent control over the phase and amplitude of each resonator is not available in metasurface antenna designs [41], metasurfaces instead rely on the phase advance of the feed wave combined with the tuning state of the elements to provide beamforming capabilities. Instead, the weights for metasurface can be represented in the array factor calculation as[41]:

$$AF(\phi_0) = \sum_{n=1}^{N} A_m(\omega)e^{-jk_0 y_m \sin(\phi_0)}e^{-j\beta y_m}. \quad (4)$$

When this factor is multiplied by the individual element's radiation pattern[42][43], the ideal result is a directive beam in the far-field. In this model, y_m is the position along the aperture, k_0 and $\beta$are the wavenumbers of free space and the feed wave, ω is the frequency, N is the number of elements, and ϕ_0 is the desired beam angle. This equation can be solved for the elements' complex weighting factors, A_m, which can be enforced to achieve the desired pattern.

Based on the previous equations and calculations, a conformal metasurface antenna system is proposed. The proposed conformal metasurface antenna system consists of two parts: 1. The conformal metasurface, and 2. the Conventional patch antenna. As shown in Figure 6, a conformal

metasurface is placed near a conventional patch antenna. The conformal surface acts as a reflector of a patch antenna. With radio waves traveling with different distances and angles, the conformal metasurface is divided into multiple subwavelength segments. The angle transformation from conformal into planar waves can be based on the geometric method. The shortest distance in a desired direction can be used as a reference, i.e. R_0+S_0. The phase difference between ray S_1 and S_2 can be regarded as [40]:

$$\Delta\varphi=k_0[(|R_1|+|S_1|) - (|R_0|+|S_0|)] \quad (5)$$

where $\Delta\varphi$ is the phase difference and k_0 is the free-space wave vector. From (1) the phase difference can be controlled by manipulating the distance of different waves. One way to achieve that is by changing the curvature of the metasurface. As Figure 6(b) showed, when changing the curvature of the conformal surface radius from 40 mm to 88mm, the direction of the beam is expected to change.

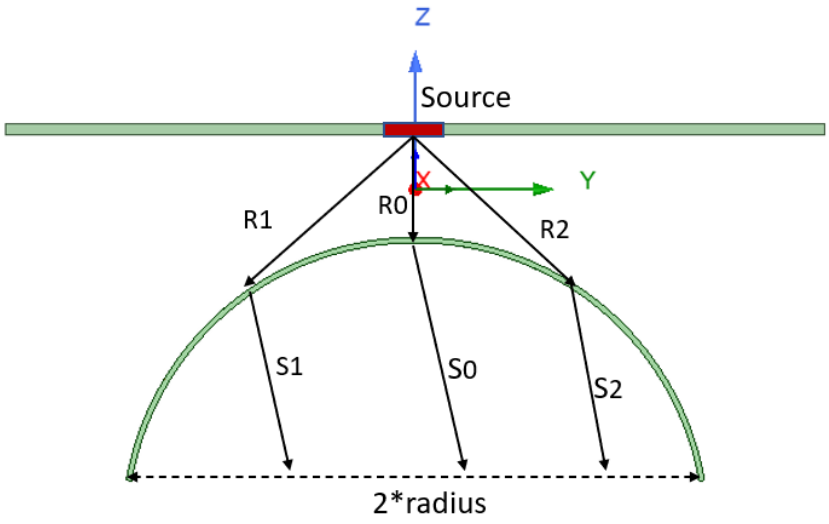

(a)

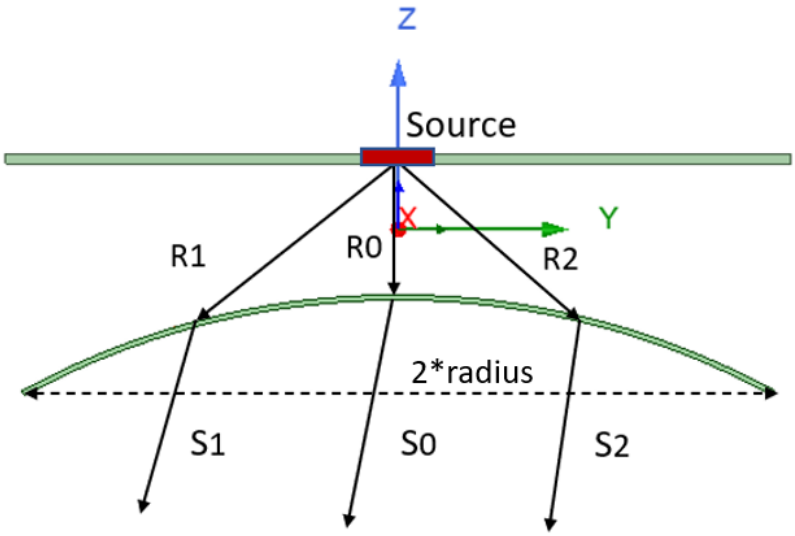

(b)

Figure 6. Conformal metasurface antenna proposal: (a) proposed conformal metasurface with radius of 40mm. (b) proposed conformal metasurface with radius of 88 mm.

2.2. Proposed conformal metasurface antenna system

To further verify this design idea, simulations are performed using the finite element solver HFSS. The layout of the patch antenna and metasurface is show in the Figures 7 and 8. Figure 7(a) showed the layout of the conventional patch antenna. This patch antenna is designed with a center frequency of 2.4 GHz and is printed on a 1.6 mm thick FR4 substrate with dielectric constant of 4.04[44]. The goal here is to have the most conventional and cost-effective patch antenna to verify

the effectiveness of the conformal metasurface. The substrate size is designed as the same size of the conformal metasurface path. The layout of the conformal metasurface is presented in Figure 8(a). The layout consisted of a 5x5 unit cell square with a size of 18mm. The overall length of the substrate was 120mm. The gap between each unit square was 1 mm.

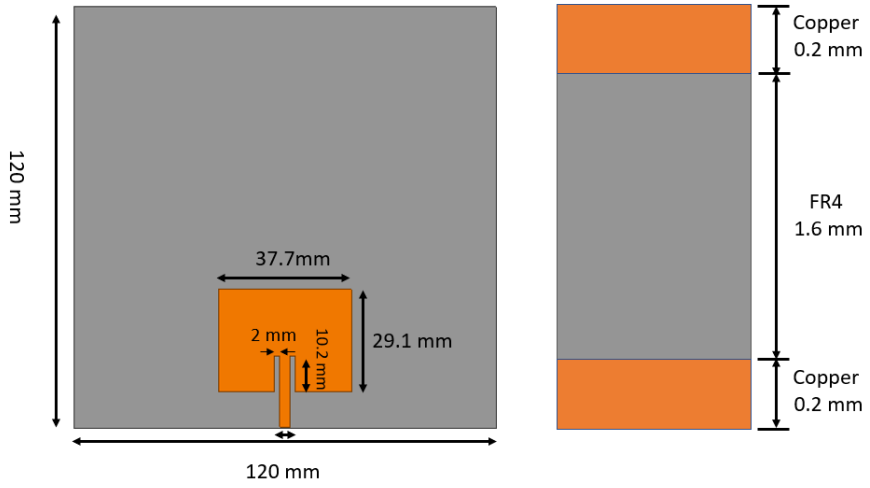

(a) (b)

Figure 7. Patch antenna layout (a) top view; (b) side view.

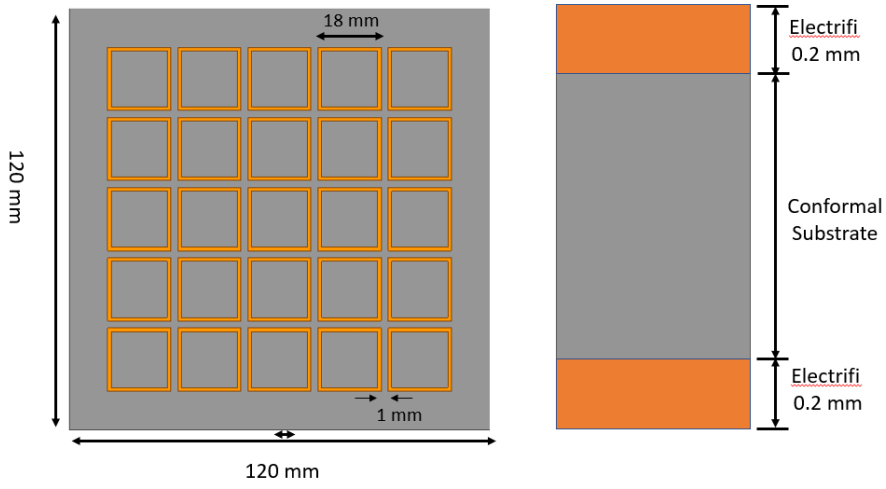

(a) (b)

Figure 8. Conformal metasurface layout (a) top view ; (b) side view.

Three different conformal materials have been simulated as substrate: 1. Rogers 5870 conformal metasurface, 2. 3D Printing Ninja flex conformal metasurface, and 3. Panasonic Felios F775 flexible PCB conformal metasurface. With each material came a different permittivity value and firmness of the substrate. The specific property comparison of the conformal materials is shown at the Table 1.

Table 1. Properties comparison of the conformal material.

Material	Permitivity
Rogers 5870	2.33 [45]
3d Printing Ninja Flex	3.7 [46]
Panasonic Felios F775	3.2 [47]

2.3. HFSS simulation result

The objective of this dissertation is to explore the influences of conformal metasurfaces on passive beam steering. To have a better understanding, three conformal materials are simulated. While those materials have different permittivity, all the other physical de-sign parameters stay the same. The radius of the conformal metasurface is changed from 43 mm to 83 mm.

As shown in Figure 9, for the Rogers 5870 conformal metasurface, the overall gain increased from 1.12 dB to 3.718 dB. The phase difference between the 43mm radius and 88 mm radius is 25 degrees. Figure 10 shows the simulation results of the Ninja Flex metasurface influence. Ninja flex is a 3D printing material that can be used as a substrate for an antenna. Previous research [46] demonstrates that this can be used as a substrate for a patch antenna. The overall gain was increased from 1.31 dB to 3.12 dB when the radius changed from 43mm to 88 mm. And the phase difference between the largest and smallest radius was 19 degrees. Figure 11 shows the simulation results of the Panasonic Felios F775 conformal metasurface influence. The

overall gain was increased from 1.26 dB to 2.51 dB when the radius changed from 43mm to 88 mm.

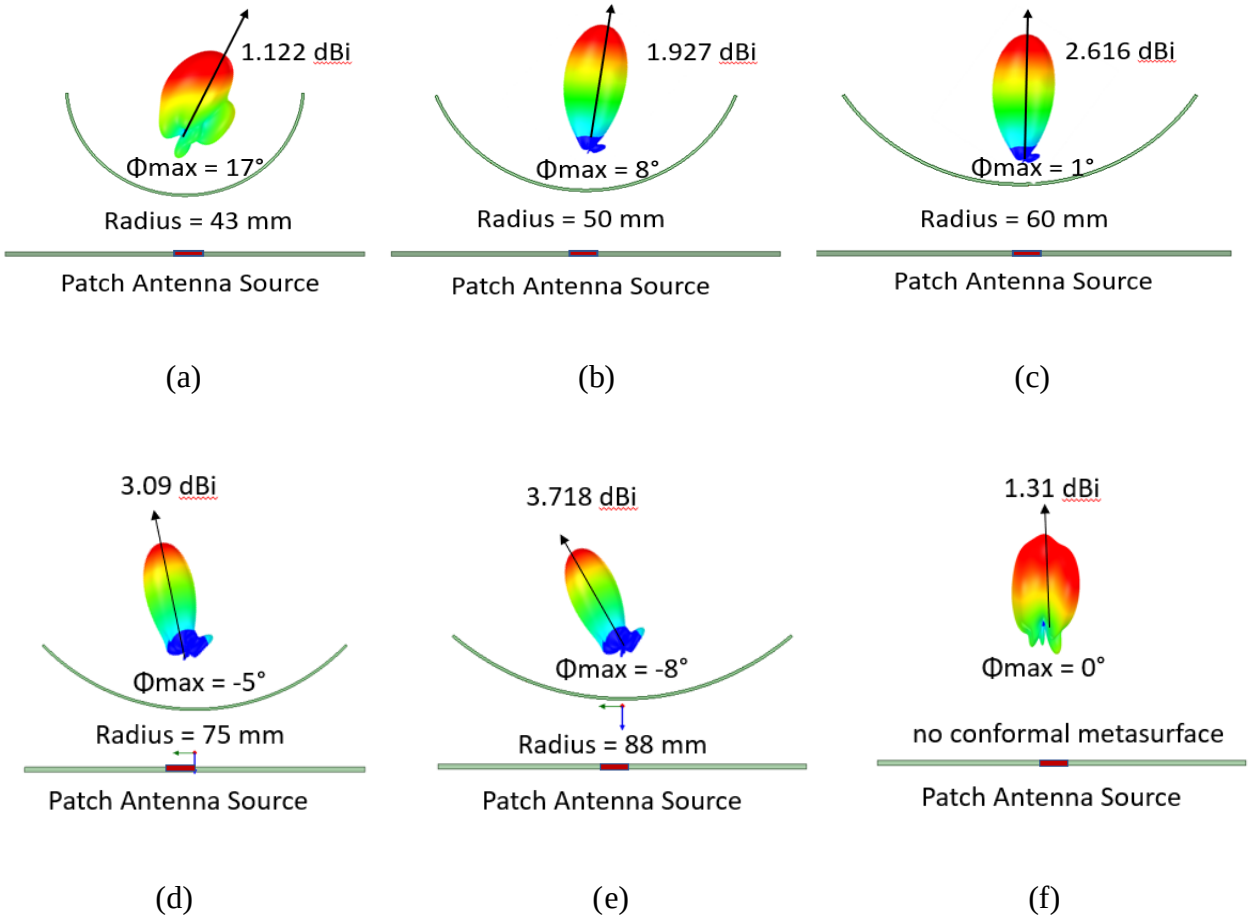

Figure 9. Simulation result: comparison of different radius for Rogers 5870 conformal metasurface on patch antenna at 2.45 GHz. (a) r = 43 mm; (b) r = 50 mm; (c) r = 60 mm; (d) r= 75 mm; (e) r = 88 mm. (f) no conformal metasurface.

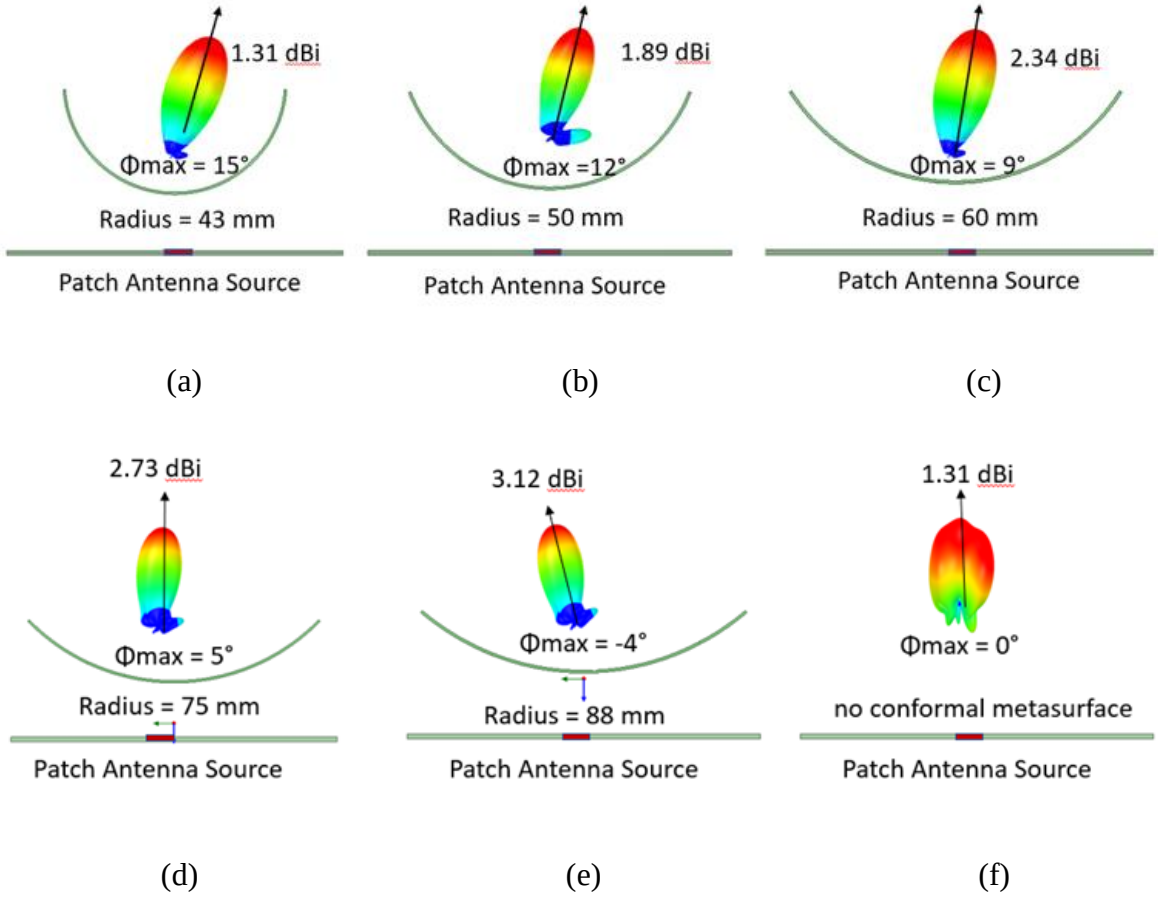

Figure 10. Effect of different radius for Ninja flex conformal metasurface on patch antenna at 2.45 GHz. (a) r = 43 mm; (b) r = 50 mm; (c) r = 60 mm; (d) r= 75 mm; (e) r = 88 mm. (f) no conformal metasurface.

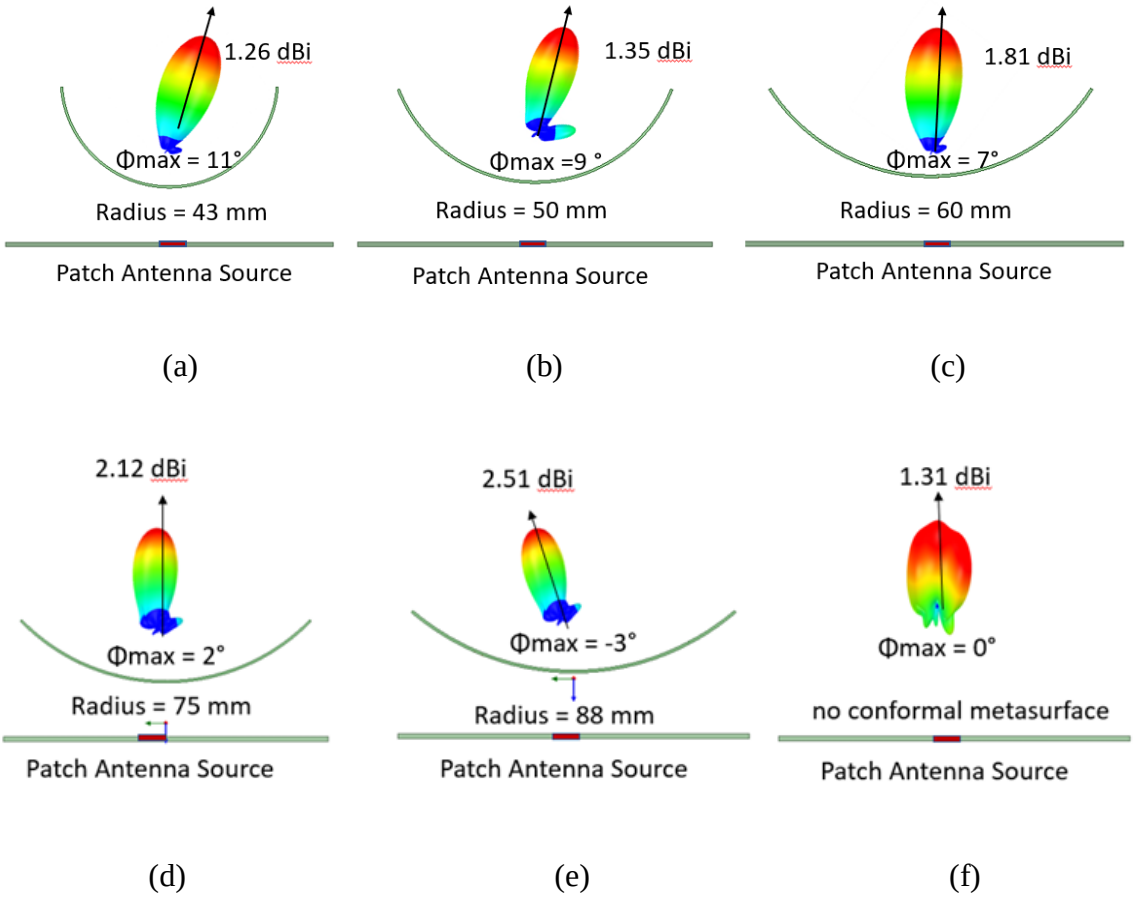

Figure 11. Effect of different radius for Panasonic Felios F775 conformal metasurface on patch antenna at 2.45 GHz. (a) r = 43 mm; (b) r = 50 mm; (c) r = 60 mm; (d) r= 75 mm; (e) r = 88 mm. (f) no conformal metasurface.

Comparing three different materials, it's shown that the overall gain increased when the radius of the conformal surface increased. When the conformal metasurface was not placed near the patch antenna, the overall gain was shown to be 1.31 dB, when adding the conformal metasurface, the overall gain was increase and phase has been shifted.

Overall, the Rogers 5870 conformal metasurface is shown to have a better ability to shift the phase while the Panasoic felios F775 had the lowest in simulation. On the other hand, the Panasoic felios F775 had the best ability to bend, while Rogers is more difficult to bend than the other two.

3. FABRICATION AND MEASUREMENT

3.1. Fabrication

There are many materials and techniques that can be utilized to fabricate metasurfaces. Most of those materials and techniques can be divided into three categories: all-dielectric, printed layers, and all-metal. All-dielectric metasurfaces were fabricated by low loss and high permittivity dielectric structures [48]. It was utilized for many applications such as broadband optical beam splitters [49], electromagnetic band gap (EBG) resonator antennas [50], and ultralow profile lens antenna [51].

A metasurface can also be made of printed materials as explained in [52]. Printed layer metasurfaces are known for their low cost and fast prototyping time for complex structures. Studies such as [53] demonstrated the wide adaptability for low-cost projects. There are also some studies utilizing all-metal structures such as [54]. In this paper, in-expensive thin layers of metal sheets were used to fabricate frequency-selective surfaces(FSS), and those surfaces could be manufactured in large quantities with low cost.

In this work, the goal is to explore different conformal metasurfaces for passive beam steering. Most applications for passive beam steering require fast prototyping times and relative low costs. While conformal antennas are easy to manipulate gain by changing their shape, they are harder to manufacture than traditional patch antennas. In this work, three manufacture methods have been utilized to manufacture the conformal metasurface. The Rogers 5870 conformal metasurface was fabricated by a laser direct etching method. The Ninja flex conformal metasurface was fabricated by 3D printing. The Panasoic felios F775 was a flex pcb material.

For the Rogers 5870 conformal metasurface shown in Figure12(a), a laser-direct engraving method was used to fabricate it. The conductive layer was etched away, leaving only designed square rings on the surface. A LPFK laser engraving machine was used for this printing.

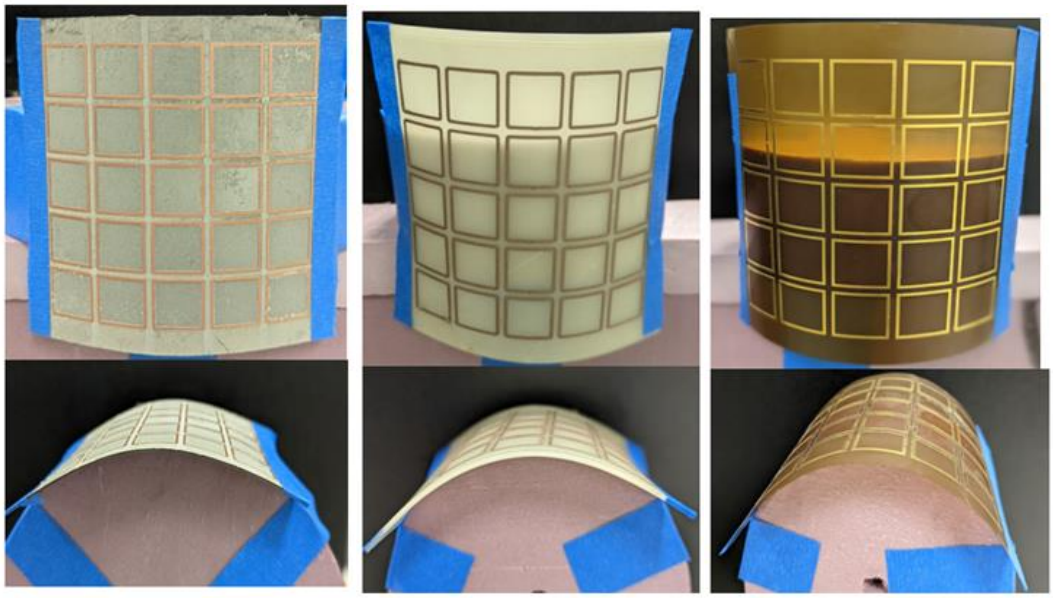

(a) (b) (c)

Figure 12. Fabricated conformal metasurface (a) laser-direct engraving Rogers 5870; (b) 3D printed NinjaFlex; (c) The Panasoic Felios F775 flexible PCB.

The thickness of this antenna was 0.7874mm (0.031 inch) which made the metasurface conformal. There are some challenges that come with this method. Mainly the surface area is large, some of the surface area is not totally smooth, but it shouldn't influence the performance of the conformal metasurface.

The ninja flex 3D printed conformal metasurface is shown in the Figure12(b). Additive manufacturing by 3D printing has made a lot of progress recently [55-57]. The growing demands for low-cost and complex 3D structures makes 3D printing a great option for many researchers. NinjiaFlex is a flexible 3D printing filament which allows for conformal surfaces to be fabricated by a 3D printer. Previous research [46] indicates it can be a good substrate material for conformal

surfaces. The permittivity of the material was reported as 3.7 [46]. For the 3D printing process, the infill is set as 100% to get a better result. The squareconductors for designed ring are Electrifi. As discussed in [62], utilizing NinjaFlex and Electrifi to print this design requires great care due to the difference in filament extrusion temperatures. Furthermore, Electrifi conducting filament loses some of its conductivity when dispensed at higher temperatures. However, when a lower print temperature is used, extrusion is inconsistent and may produce voids (open circuits).

To achieve high quality extrusion at low temperatures, the factory default print nozzle (0.4 mm) was replaced with a larger 1.0 mm diameter nozzle, and the extrusion temperature was reduced to 160 °C. To print at this lower temperature, g-code command M302 P1 was used to disable the printer's cold extrusion checking.

The Panasoic felios F775 conformal metasurface is shown in the Figure 12(c). Compared with the other two materials, this conformal metasurface has the best ability to bend. The prototype is outsourced to Oshpark which is very cost effective. This printed design sample comes with great uniformity for the substrate and shows a great potential.

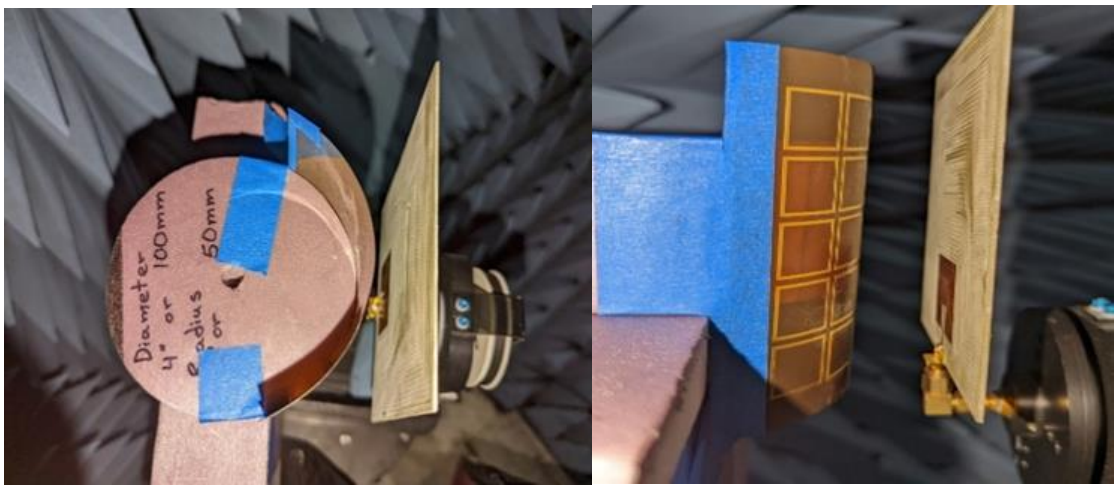

(a) (b)

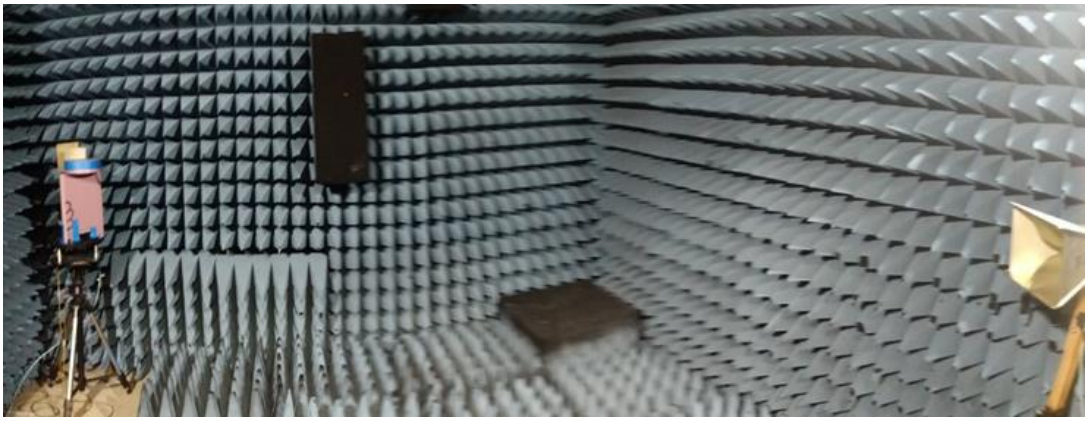

(c)

Figure 13. Measurement setup (a) conformal surface top view. (b) conformal surface side view. (c) measurement setup.

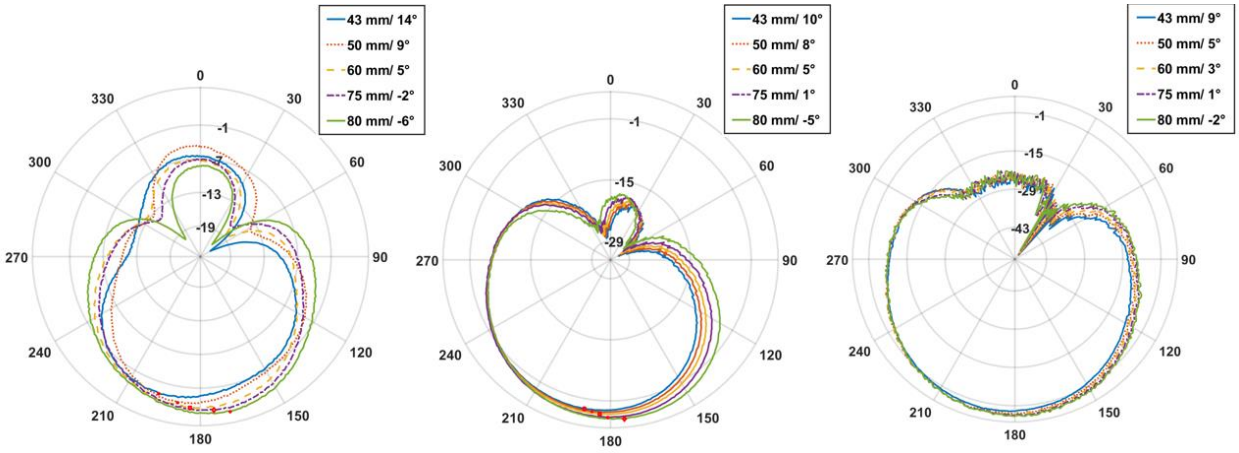

(a) (b) (c)

Figure 14. Radiation pattern of far field gain for conformal metasurface (a) Rogers 5870. (b) Ninjaflex 3D printing. (c) Panasoic Felios F775 flexible PCB.

3.2. Measurement setup and result

The measurements were performed in an anechoic chamber. To test the conformal metasurface prototype's influence on the patch antenna, support surfaces of various radius were fabricated. The Styrofoam was cut as disks, this extruded polystyrene was chosen for uniformly fine grain, rigidity, and low density. This material has a relative dielectric constant in the range of 1.02 to 1.04, which make them close to the dielectric value of free space. It is important to make the cylindrical object surface as smooth as possible since the conformal metasurface is attached to the cylindrical object. The patch antenna and conformal metasurface were fixed with the turntable so they always faced each other. A reference horn antenna was placed in the far-field range as a the transmit antenna as shown in Figure 13. There was a 20 mm fixed distance set between the patch antenna and conformal metasurface. The far-field gain measurement was then per-formed for each metasurface with different radius varied from 43 mm to 88 mm. Figures 14 shows the simulation results of the far field radiation pattern for three materials as a comparison to the measured result

Figure 15a shows the measured far field radiation pattern for the Rogers 5870 conformal metasurface at 2.4 GHhz . The gain increased from 1.21 dB to 3.47 dB when the radius increased from 43 mm to 88 mm. The main beam was steered from 14° to −6°. A 20° phase shifting was achieved. Figure 15b shows the far field radiation pattern for the Ninja Flex conformal metasurface at 2.4 GHhz. The gain increased from 1.38 dB to 2.89 dB when the radius increased from 43 mm to 88 mm. The main beam was steered from 10° to −5°. Figure 14c shows the far field radiation pattern for Panasoic Felios F775 flexible PCB conformal metasurface at 2.4 GHhz. The gain increased from 1.13 dB to 2.31 dB when the radius increased from 43 mm to 88 mm. The main beam was steered from 9° to −2°. A simulation result and measurement comparison were shown in Figures 14. There is a good agreement between the simulation and measurement results.

Table 2 shows the gain and phase comparison between each material. This table also indicated a good agreement between the measurement and simulation results. The above simulation and measurement results verified the effectiveness of the passive conformal metasurface.

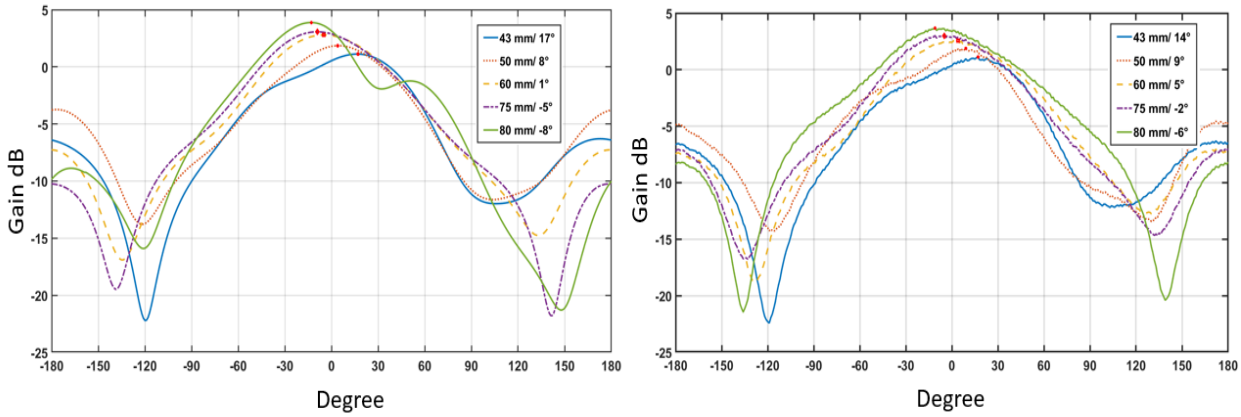

(a)

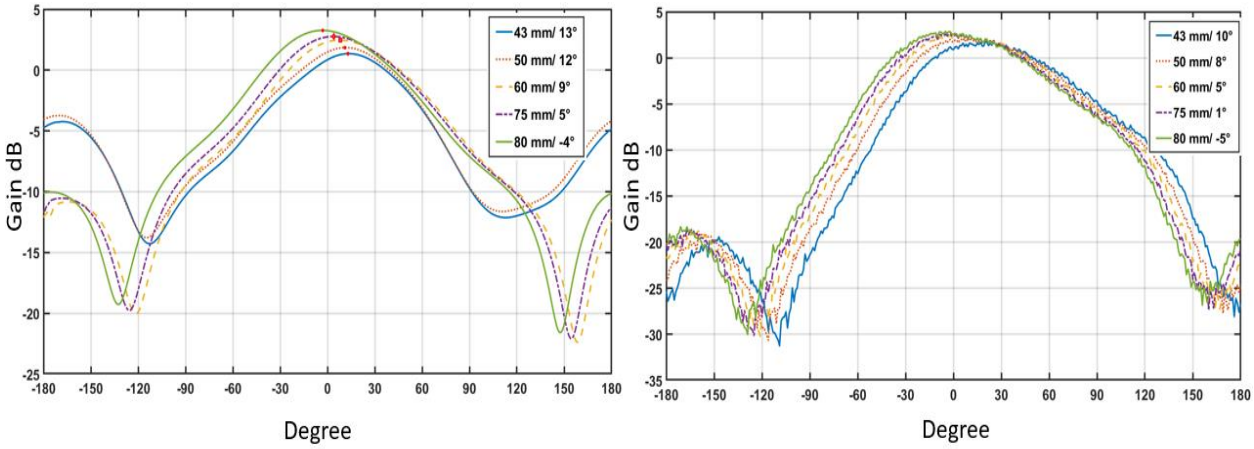

(b)

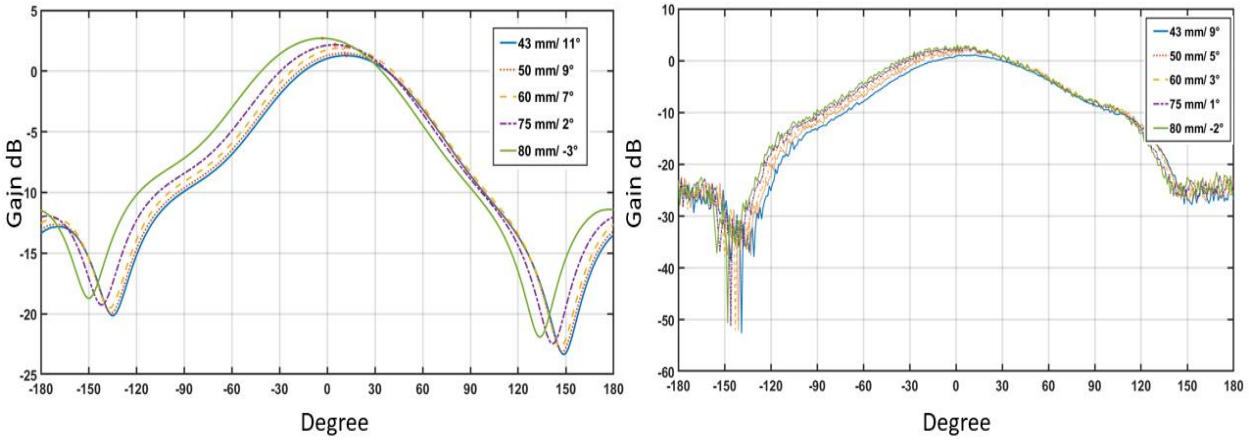

(c)

Figure 15. Far field radiation pattern rectangular plot comparison for conformal metasurface. (a) Rogers 5870. (b) Ninjaflex 3D printing. (c) Panasoic Felios F775 flexible PCB.

Table 2. Simulation and measurement result for gain and phase.

Material	Radius	Simulated G_{max}	Measured G_{max}	Simulated P_{max}	Measured P_{max}
Rogers 5870	43 mm	1.122 dB	1.21 dB	17°	14°
	50 mm	1.927 dB	1.86 dB	8°	9°
	60 mm	2.616 dB	2.53 dB	1°	5°
	75 mm	3.09 dB	2.98 dB	-5°	2°
	88 mm	3.718 dB	3.47 dB	-8°	-6°
NinjaFlex	43 mm	1.31 dB	1.38 dB	13°	10°
	50 mm	1.89 dB	1.74 dB	12°	8°
	60 mm	2.34 dB	2.14 dB	9°	5°
	75 mm	2.73 dB	2.76 dB	5°	1°
	88 mm	3.12 dB	2.89 dB	-4°	-5°
Panasoic felios	43 mm	1.26 dB	1.13 dB	11°	9°
	50 mm	1.35 dB	1.31 dB	9°	5°
	60 mm	1.81 dB	1.74 dB	7°	3°
	75 mm	2.12 dB	2.07 dB	2°	1°
	88 mm	2.51 dB	2.31 dB	-3°	-2°

The purpose of this work is to experimentally explor different conformal materials for beam shifting and gain improvement. The conventional patch antenna used here was a very common 2.4 GHz FR4 patch antenna with low cost. The overall gain without the conformal metasurface was about 1.31 dB. By simply placing a passive conformal metasurface at a fixed distance, the main lobe of the patch antenna was shifted. Furthermore, beam shifting could be changed by increasing the radius of the conformal metasurface. Comparing the measurement results of the three prototypes, the Rogers 5870 substrate had the highest gain improvement of 2.26 dB. The max phase angle also shifted 20° when changing the radius from 43 mm to 88 mm. Ninja Flex had a 1.41 dB gain improvement and 15° beam shifting. Panasoic Felios had a 1.18 dB gain improvement and the max phase angle shifted 11°. On the other hand, Panasoic Felios is the most flexible one among the three fabricated conformal metasurfaces. It is a good option for gain

improvement of compact antenna designs. Three different manufacturing methods were explored for each conformal metasurface material. Ninja Flex 3D printing material had a lower cost compared to the Rogers 5870 substrate making it a good option for fast prototyping. It also came with challenges to adjust temperatures in case losing the conductivity of Electrifi.

Compared with active conformal metasurface, which the beam can shift up to 60 degrees [34], this passive conformal metasurface has narrower beam shifting ability up to 20 degrees. However, active conformal metasurfaces rely on phase control circuitry and beamforming networks interrelated with active phase shifters. Passive conformal metasurface is more cost effective, simpler to manufacture and easier to integrate.

To improve related research in the future, more complex structure such as antenna array can be added as radiating elements to improve the overall gain. The conformal metasurface can extract as a model for future research. Furthermore, the relationship between the side lobe and radius when bending can be further studied.

4. CONCLUSION

In conclusion, this work demonstrated that the conformal metasurface can be used to steer the beam from a conventional patch antenna without using active phase shifters, a beamforming network, or complex structures for the first time. The proposed passive conformal metasurface was placed near a conventional patch antenna as a parasitic surface. Three conformal materials have been experimentally evaluated to demonstrate the beam steering ability and efficiency. The proposed designs have been simulated, fabricated, and measured. The radiation pattern shows up to a 20° phase shift. Furthermore, different fabrication methods have been explored. The proposed approach can be further extended to higher frequencies, enabling future work such as low power consumption millimeter wave beam steering systems.

REFERENCES

1. J. G. Andrews et al., “What will 5G be?” IEEE J. Sel. Areas Commun., vol. 32, no. 6, pp. 1065–1082.

2. K. Benson, “Phased array beamforming ICs simplify antenna design,” Analog Dialogue, vol. 53, no. 1, pp. 10-13, 2019, [Online] Available: https://www.analog.com/en/analog-dialogue/articles/phased-arraybeamforming-ics-simplify-antenna-design.html.

3. A. Navarro and K. Chang, Integrated Active Antennas and Spatial Power Combining. New York, NY, USA: Wiley, 1996.

4. W. Yan, X. Yuan, Z. -Q. He and X. Kuai, "Passive Beamforming and Information Transfer Design for Reconfigurable Intelligent Surfaces Aided Multiuser MIMO Systems," in IEEE Journal on Selected Areas in Communications, vol. 38, no. 8, pp. 1793-1808. 2013.

5. S. Hu, F. Rusek, and O. Edfors, “Beyond massive MIMO: The potential of data transmission with large intelligent surfaces,” IEEE Trans. Signal Process., vol. 66, no. 10, pp. 2746–2758, May 2018.

6. Q. Zhang, H. Guo, Y.-C. Liang, and X. Yuan, “Constellation learningbased signal detection for ambient backscatter communication systems,” IEEE J. Sel. Areas Commun., vol. 37, no. 2, pp. 452–463, Feb. 2019

7. X. Wan, M. Q. Qi, T. Y. Chen, and T. J. Cui, ‘‘Field-programmable beam reconfiguring based on digitally-controlled coding metasurface,’’ Sci. Rep., vol. 6, Feb. 2016, Art. no. 20663.

8. L. Zhang, X. Q. Chen, S. Liu, Q. Zhang, J. Zhao, J. Y. Dai, G. D. Bai, X. Wan, Q. Cheng, G. Castaldi, V. Galdi, and T. J. Cui, ‘‘Space-time-coding digital metasurfaces,’’ Nature Commun., vol. 9, pp. 1–11, Oct. 2018.

9. A. Pal, A. Mehta, H. Goonesinghe, D. Mirshekar-Syahkal and H. Nakano, "Conformal Beam-Steering Antenna Controlled by a Raspberry Pi for Sustained High-Throughput Applications," in *IEEE Transactions on Antennas and Propagation*, vol. 66, no. 2, pp. 918-926, Feb. 2018.

10. M. R. M. Hashemi, S.-H. Yang, T. Y. Wang, N. Sepúlveda, and M. Jarrahi, ‘‘Electronically-controlled beam-steering through vanadium dioxide metasurfaces,’’ Sci. Rep., vol. 6, Oct. 2016, Art. no. 35439.

11. B. Orazbayev, M. Beruete, and I. Khromova, ‘‘Tunable beam steering enabled by graphene metamaterials,’’ Opt. Express, vol. 24, no. 8, pp. 8848–8861, Apr. 2016.

12. T. J. Cui, M. Q. Qi, X. Wan, J. Zhao, and Q. Cheng, ‘‘Coding metamaterials, digital metamaterials and programmable metamaterials,’’ Light, Sci. Appl., vol. 3, pp. 1–9, Oct. 2014.

13. S. Liu and T. J. Cui, ‘‘Concepts, working principles, and applications of coding and programmable metamaterials,’’ Adv. Opt. Mater., vol. 5, no. 22, Nov. 2017, Art. no. 1700624.

14. Zhu, W.M.; Liu, A.Q.; Zhang, W.; Tao, J.F.; Bourouina, T.; Teng, J.H.; Zhang, X.H.; Wu, Q.Y.; Tanoto, H.; Guo, H.C.; et al. Polarization dependent state to polarization independent state change in THz metamaterials. Appl. Phys. Lett.

15. Pitchappa, P.; Ho, C.P.; Dhakar, L.; Lee, C. Microelectromechanically reconfigurable interpixelated metamaterial for independent tuning of multiple resonances at terahertz spectral region. *Optica* **2015**, *2*, 571–578.

16. P. -Y. Qin, L. -z. Song and Y. J. Guo, "Beam Steering Conformal Transmitarray Employing Ultra-Thin Triple-Layer Slot Elements," in *IEEE Transactions on Antennas and Propagation*, vol. 67, no. 8, pp. 5390-5398, Aug. 2019.

17. Y. F. Wu and Y. J. Cheng, "Proactive Conformal Antenna Array for Near-Field Beam Focusing and Steering Based on Curved Substrate Integrated Waveguide," in *IEEE Transactions on Antennas and Propagation*, vol. 67, no. 4, pp. 2354-2363, April 2019.

18. S. Shi et al., "Conformal Wideband Optically Addressed Transmitting Phased Array With Photonic Receiver," in Journal of Lightwave Technology, vol. 32, no. 20, pp. 3468-3477, 15 Oct.15, 2014

19. G. -L. Huang, J. Li, T. Yuan and C. -Y. -D. Sim, "Recent Progress in Practical Waveguide-Based Antennas and Passive Components With Additive Manufacturing Technology," 2018 IEEE Asia-Pacific Conference on Antennas and Propagation (APCAP), 2018, pp. 70-71

20. A. I. Zaghloul and O. Kilic, "Hybrid Beam Former for Distributed-Aperture Electronically Steered Arrays," in *IEEE Antennas and Wireless Propagation Letters*, vol. 9, pp. 678-681, 2010.

21. C. Huang, W. Pan, X. Ma, B. Zhao, J. Cui and X. Luo, "Using Reconfigurable Transmitarray to Achieve Beam-Steering and Polarization Manipulation Applications," in *IEEE Transactions on Antennas and Propagation*, vol. 63, no. 11, pp. 4801-4810, Nov. 2015.

22. K. Singh, M. U. Afzal, M. Kovaleva and K. P. Esselle, "Controlling the Most Significant Grating Lobes in Two-Dimensional Beam-Steering Systems With Phase-Gradient Metasurfaces," in *IEEE Transactions on Antennas and Propagation*, vol. 68, no. 3, pp. 1389-1401, March 2020.

23. F.H. Lin and Z. N. Chen, "Low-Profile Wideband Metasurface Antennas Using Characteristic Mode Analysis," in IEEE Tranactions on Antennas and Propagation, vol. 65, no. 4, pp. 1706-1713, April 2017.

24. Q. Nguyen and A. I. Zaghloul, "Design of Beam Steering Patch Arrays Using Self-Phased Metasurface Pixels," 2020 IEEE International Symposium on Antennas and Propagation and North American Radio Science Meeting, 2020, pp. 909-910.

25. J. P. Turpin, J. A. Bossard, K. L Morgan, D. H. Werner, and P. L. Werner, "Reconfigurable and tunable metamaterials: a review of the theory and applications," International Journal of Antennas and Propagation, 2014.

26. J. Wang *et al*., "Metantenna: When Metasurface Meets Antenna Again," in *IEEE Transactions on Antennas and Propagation,* vol. 68, no. 3, pp. 1332-1347, March 2020.

27. T. Cai *et al*., "Ultra-Thin Polarization Beam Splitter Using 2-D Transmissive Phase Gradient Metasurface," in *IEEE Transactions on Antennas and Propagation*, vol. 63, no. 12, pp. 5629-5636, Dec. 2015.

28. Lalbakhsh, A.; Esselle, K.P. Directivity Improvement of a Fabry-Perot Cavity Antenna by Enhancing Near Field Charac-Teristic. In Proceedings of the 2016 17th International Symposium on Antenna Technology and Applied Electromagnetics (ANTEM), Montreal, QC, Canada, 10–13 July 2016; pp. 1–2

29. Lalbakhsh, A.; Afzal, M.U.; Esselle, K.P.; Smith, S.; Zeb, B.A. Single-Dielectric Wideband Partially Reflecting Surface with Variable Reflection Components for Realization of a Compact High-Gain Resonant Cavity Antenna. *IEEE Trans. Antennas Propag.* **2019**, *67*, 1916–1921.

30. Lalbakhsh, A.; Afzal, M.U.; Esselle, K.P. Multiobjective Particle Swarm Optimization to Design a Time-Delay Equalizer Metasurface for an Electromagnetic Band-Gap Resonator Antenna. IEEE Antennas Wirel. Propag. Lett. 2017, 16, 912–915.

31. Das, P.; Mandal, K.; Lalbakhsh, A. Single-layer polarization-insensitive frequency selective surface for beam reconfigurability of monopole antennas. J. Electromagn. Waves Appl. 2020, 34, 86–102.

32. Lalbakhsh, A.; Afzal, M.U.; Esselle, K.P.; Smith, S. Design of an Artificial Magnetic Conductor Surface Using an Evolutionary Algorithm. In Proceedings of the 2017 International Conference on Electromagnetics in Advanced Applications (ICEAA), Verona, Italy, 11–15 September 2017; pp. 885–887.

33. Paul, G.S.; Mandal, K.; Lalbakhsh, A. Single-layer ultra-wide stop-band frequency selective surface using inter-connected square rings. *Aeu-Int. J. Electron. Commun.* **2021**, *132*, 153630.

34. Lalbakhsh, A.; Afzal, M.U.; Hayat, T.; Esselle, K.P.; Mandal, K. All-metal wideband metasurface for near-field transformation of medium-to-high gain electromagnetic sources. Sci. Rep. 2021, 11, 9421.

35. H. L. Zhu, X. H. Liu, S. W. Cheung and T. I. Yuk, "Frequency-Reconfigurable Antenna Using Metasurface," in *IEEE Transactions on Antennas and Propagation*, vol. 62, no. 1, pp. 80-85, Jan. 2014.

36. W. E. I. Liu, Z. N. Chen, X. Qing, J. Shi and F. H. Lin, "Miniaturized Wideband Metasurface Antennas," in *IEEE Transactions on Antennas and Propagation*, vol. 65, no. 12, pp. 7345-7349, Dec. 2017

37. M. U. Afzal and K. P. Esselle, "Steering the Beam of Medium-to-High Gain Antennas Using Near-Field Phase Transformation," in IEEE Transactions on Antennas and Propagation, vol. 65, no. 4, pp. 1680-1690, April 2017.

38. Y. -B. Kim, S. Lim and H. L. Lee, "Electrically Conformal Antenna Array With Planar Multipole Structure for 2-D Wide Angle Beam Steering," in *IEEE Access*, vol. 8, pp. 157261-157269, 2020.

39. B. D. Braaten, S. Roy, I. Irfanullah, S. Nariyal and D. E. Anagnostou, "Phase-Compensated Conformal Antennas for Changing Spherical Surfaces," in *IEEE Transactions on Antennas and Propagation*, vol. 62, no. 4, pp. 1880-1887, April 2014.

40. Li, H.; Ma, C.; Shen, F.; Xu, K.; Ye, D.; Huangfu, J.; Li, C.; Ran, L.; Denidni, T.A. Wide-Angle Beam Steering Based on an Active Conformal Metasurface Lens. IEEE Access 2019, 7, 185264–185272.

41. T. Sleasman *et al*., "Experimental Synthetic Aperture Radar With Dynamic Metasurfaces," in *IEEE Transactions on Antennas and Propagation*, vol. 65, no. 12, pp. 6864-6877, Dec. 2017

42. C. A. Balanis, Antenna Theory: Analysis and Design, vol. 1. Hoboken, NJ, USA: Wiley, 2005.

43. L. M. Pulido-Mancera, T. Zvolensky, M. F. Imani, P. T. Bowen, M. Valayil, and D. R. Smith, “Discrete dipole approximation applied to highly directive slotted waveguide antennas,” IEEE Antennas Wireless Propag. Lett., vol. 15, pp. 1823–1826, 2016.

44. Isola group. Available online: https://www.isola-group.com/pcb-laminates-prepreg/370hr-laminate-prepreg/ (accessed on 2 December 2021).

45. Rogers Corporation. Available online: https://rogerscorp.com/-/media/project/rogerscorp/documents/advanced-electronics-solutions/english/data-sheets/rt-duroid-5870---5880-data-sheet.pdf /(accessed on 2 December 2021).

46. R. Striker, D. Mitra and B. D. Braaten, "Permittivity of 3D Printed NinjaFlex Filament for use in Conformal Antenna Designs up to 20 GHz," 2020 IEEE International Conference on Electro Information Technology (EIT), 2020, pp. 224-227

47. Panasonic Corporation. Available online: https://docs.oshpark.com/resources/flex-substrate-Panasonic-Felios-F775.pdf/(accessed on 2 December 2021).

48. Monti, A.; Alu, A.; Toscano, A.; Bilotti, F. Surface Impedance Modeling of All-Dielectric Metasurfaces. *IEEE Trans. Antennas Propag.* **2019**, *68*, 1799–1811.

49. Lalbakhsh, A.; Esselle, K.P. Directivity Improvement of a Fabry-Perot Cavity Antenna by Enhancing Near Field Charac-Teristic. In Proceedings of the 2016 17th International Symposium on Antenna Technology and Applied Electromagnetics (ANTEM), Montreal, QC, Canada, 10–13 July 2016; pp. 1–2.

50. Lalbakhsh, A.; Afzal, M.; Esselle, K.; Smith, S. A High-Gain Wideband EBG Resonator Antenna for 60 GHz Unlicenced Frequency Band. In Proceedings of the 12th European Conference on Antennas and Propagation (EuCAP 2018), London, UK, 9–13 April 2018.

51. Wang, Z.; Wu, H.; Chen, J.; Wu, Z.; Feng, Y. An ultralow-profile lens antenna based on all-dielectric metasur-faces. In Proceedings of the 2016 IEEE 5th Asia-Pacific Conference on Antennas and Propagation (APCAP), Kaohsiung, Taiwan, 26–29 July 2016, pp. 367–368.

52. Adibi, S.; Honarvar, M.A.; Lalbakhsh, A. Gain Enhancement of Wideband Circularly Polarized UWB Antenna Using FSS. *Radio Sci.* **2020**, *56*, 1–8.

53. Afzal, M.U.; Matekovits, L.; Esselle, K.P.; Lalbakhsh, A Beam-Scanning Antenna Based on Near-Electric Field Phase Transformation and Refraction of Electromagnetic Wave Through Dielectric Structures. *IEEE Access* **2020**, *8*, 199242–199253.

54. Lalbakhsh, A.; Afzal, M.U.; Esselle, K.P.; Smith, S.L. All-Metal Wideband Frequency-Selective Surface Bandpass Filter for TE and TM polarizations. IEEE Trans. Antennas Propag. 2022, PP, 1. https://doi.org/10.1109/tap.2021.3138256.

55. Zhang, S.; Cadman, D.; Vardaxoglou, J.Y.C. Additively Manufactured Profiled Conical Horn Antenna with Dielectric Loading. *IEEE Antennas Wirel. Propag. Lett.* **2018**, *17*, 2128–2132.

56. Dorle, A.; Gillard, R.; Menargues, E.; Van Der Vorst, M.; De Rijk, E.; Martin-Iglesias, P.; Garcia-Vigueras, M. Additive Manufacturing of Modulated Triple-Ridge Leaky-Wave Antenna. *IEEE Antennas Wirel. Propag. Lett.* **2018**, *17*, 2123–2127.

57. Su, Z.; Klionovski, K.; Bilal, R.M.; Shamim, A. A Dual Band Additively Manufactured 3-D Antenna on Package with Near-Isotropic Radiation Pattern. *IEEE Trans. Antennas Propag.* **2018**, *66*, 3295–3305.

58. V. Gjokaj, J. Papapolymerou, J. D. Albrecht, B. Wright and P. Chahal, "A Compact Receive Module in 3-D Printed Vivaldi Antenna," in *IEEE Transactions on Components, Packaging and Manufacturing Technology*, vol. 10, no. 2, pp. 343-346, Feb. 2020.

59. S. Zhang, D. Cadman and J. Y. C. Vardaxoglou, "Additively Manufactured Profiled Conical Horn Antenna With Dielectric Loading," in *IEEE Antennas and Wireless Propagation Letters*, vol. 17, no. 11, pp. 2128-2132, Nov. 2018.

60. A. Dorlé *et al.*, "Additive Manufacturing of Modulated Triple-Ridge Leaky-Wave Antenna," in *IEEE Antennas and Wireless Propagation Letters*, vol. 17, no. 11, pp. 2123-2127, Nov. 2018

61. Z. Su, K. Klionovski, R. M. Bilal and A. Shamim, "A Dual Band Additively Manufactured 3-D Antenna on Package With Near-Isotropic Radiation Pattern," in *IEEE Transactions on Antennas and Propagation*, vol. 66, no. 7, pp. 3295-3305, July 2018

62. S. Roy, M. B. Qureshi, S. Asif, S. Sajal, and B. D. Braaten, “A study of microstrip transmission lines on substrates created using additive manufacturing and flexible or semi-rigid filaments,” in 2017 IEEE International Conference on Electro Information Technology (EIT), 2017, pp. 200–205.